Myosin-10 and actin filaments are essential for mitotic spindle function

Sarah Woolner,[1] Lori L. O'Brien,[2] Christiane Wiese,[2] and William M. Bement[1,3]

[1]Department of Zoology, [2]Department of Biochemistry, and [3]Program in Cellular and Molecular Biology, University of Wisconsin-Madison, Madison, WI 53706

Mitotic spindles are microtubule-based structures responsible for chromosome partitioning during cell division. Although the roles of microtubules and microtubule-based motors in mitotic spindles are well established, whether or not actin filaments (F-actin) and F-actin–based motors (myosins) are required components of mitotic spindles has long been controversial. Based on the demonstration that myosin-10 (Myo10) is important for assembly of meiotic spindles, we assessed the role of this unconventional myosin, as well as F-actin, in mitotic spindles. We find that Myo10 localizes to mitotic spindle poles and is essential for proper spindle anchoring, normal spindle length, spindle pole integrity, and progression through metaphase. Furthermore, we show that F-actin localizes to mitotic spindles in dynamic cables that surround the spindle and extend between the spindle and the cortex. Remarkably, although proper anchoring depends on both F-actin and Myo10, the requirement for Myo10 in spindle pole integrity is F-actin independent, whereas F-actin and Myo10 actually play antagonistic roles in maintenance of spindle length.

Introduction

Interactions between microtubules and F-actin are a key feature of many biological processes including cell division, oogenesis, and embryonic morphogenesis (Rodriguez et al., 2003). One of the more fascinating and important examples of such interactions is provided by interaction of mitotic spindles with cortical F-actin. These interactions are required for spindle positioning in yeast (Gundersen and Bretscher, 2003; Gundersen et al., 2004) and are thought to be used for asymmetrical cell division in polarized epithelia (Perez-Moreno et al., 2003) and during orientation of the mitotic spindle in some cultured cell lines (Kaji et al., 2007; Toyoshima and Nishida, 2007). In addition, the F-actin–based motor, myosin-2, has recently been reported to exert force on spindle poles during prophase via cortical flow of anchored microtubules (Rosenblatt et al., 2004).

In the above examples, the key site of actomyosin–microtubule interaction is the cortex, and its major role is thought to be the anchoring or transport of spindle microtubules that extend there. However, whether actomyosin is an important component of the mitotic spindle interior or if actomyosin–microtubule interactions play additional roles in mitotic spindle function and assembly is the subject of an old and intense controversy. A series of fluorescence and electron microscopy studies in the 1970s described the presence of F-actin in the mitotic spindle (Schloss et al., 1977; Forer et al., 1979), and more recent work has found that various actin poisons and myosin inhibitors have varying effects on spindle structure and function (Fabian and Forer, 2007; Forer et al., 2007). However, the studies showing localization were challenged as artifacts of the methods used to prepare the samples (Barak et al., 1981), and inhibition of what was then thought to be the only metazoan actin-based motor, myosin-2, was shown to prevent cytokinesis without having any effect on spindle assembly and function (Kiehart et al., 1982). Finally, and most tellingly, morphologically normal and apparently functional spindles are routinely produced in *Xenopus laevis* egg extracts under conditions where F-actin assembly is prevented (Mitchison et al., 2005).

In contrast to mitotic spindles, meiotic spindles not only require F-actin for cortical anchoring, but, in many cases, also require F-actin for assembly (Gard et al., 1995; Kim et al., 2000; Sun et al., 2001; Sardet et al., 2002). Consistent with a role for actomyosin in the meiotic spindle, Myosin-10 (Myo10), an unconventional myosin, was recently shown to localize to meiotic spindles and to be required for their proper assembly (Weber et al., 2004). Myo10 has the unusual property of being able to bind to both F-actin, via a motor domain in its head

Correspondence to Sarah Woolner: sarah.woolner@manchester.ac.uk

S. Woolner's present address is Faculty of Life Sciences, University of Manchester, Manchester M13 9PT, UK.

Abbreviations used in this paper: HMM, heavy meromyosin; LatB, latrunculin B; MO, morpholino; Myo10, myosin-10.

The online version of this paper contains supplemental material.

The Rockefeller University Press $30.00
J. Cell Biol. Vol. 182 No. 1 77–88
www.jcb.org/cgi/doi/10.1083/jcb.200804062

(Homma et al., 2001; Homma and Ikebe, 2005); and microtubules, via a C-terminal MyTH4/FERM domain cassette (Weber et al., 2004). Intriguingly, Myo10 was also recently implicated in mitotic spindle positioning in cultured mammalian cells (Toyoshima and Nishida, 2007). Because Myo10 can bind both F-actin and microtubules, is required for meiotic spindle assembly, and is involved in mitotic spindle positioning, it is a strong candidate to mediate F-actin–microtubule interactions in mitotic spindles. We have therefore analyzed the role of both Myo10 and F-actin in mitotic spindle assembly and function in the epithelium of the vertebrate *X. laevis*. Using a combination of live cell imaging, morpholino (MO)-mediated Myo10 knockdown, and gene replacement, we show that Myo10 localizes to the mitotic spindle and is required for proper spindle anchoring, spindle pole integrity, spindle length control, and mitotic progression. Furthermore, we reveal the existence of dynamic actin cables within the mitotic spindle and show that F-actin and Myo10 play both overlapping and distinct roles during mitosis.

Results

Myo10 localizes to the poles of mitotic spindles in *X. laevis* embryos

To begin to assess a role for Myo10 in mitosis, we used immunofluorescence in early *X. laevis* embryos (stages 9–11) using an antibody directed against a small region in the head of *X. laevis* Myo10 (Weber et al., 2004). Throughout the cell cycle, Myo10 was found localized at the cell cortex (Fig. S1, available at http://www.jcb.org/cgi/content/full/jcb.200804062/DC1), as expected from previous studies (Berg et al., 2000; Berg and Cheney, 2002). In addition, during interphase, Myo10 localized to the nucleus (Fig. 1 a). However, by metaphase, Myo10 localized to the mitotic spindle, where it was found weakly associated with the entire spindle but concentrated at the spindle poles, and where it remained throughout anaphase and into telophase (Fig. 1 a). Spindle pole localization of Myo10 was also seen in spindles that were assembled in vitro from *X. laevis* egg extracts (Fig. S1). Double labeling of embryonic spindles for Myo10 and the spindle pole marker γ-tubulin showed that Myo10 localized to a region just beside the γ-tubulin domain (Fig. 1 b). The localization pattern displayed by Myo10 (in the nucleus at interphase and moving to the spindle poles during mitosis) is reminiscent of spindle assembly factors such as TPX2 and NuMA (Merdes et al., 1996; Wittmann et al., 2000). Indeed, triple labeling for α-tubulin, Myo10, and TPX2 demonstrated colocalization of Myo10 and TPX2 in the nucleus and in overlapping domains at spindle poles (Fig. 1 c).

Knockdown of Myo10 causes mitotic spindle defects

The localization pattern of Myo10 suggested that Myo10 might play a role in mitosis. To test this possibility in vivo, we used an MO knockdown approach, which has been widely used as an efficient means of gene suppression in vertebrates (Heasman, 2002). An anti-sense MO oligo was designed to target a 25-nucleotide sequence in the 5′ untranslated region and first 11 coding nucleotides of the *X. laevis* Myo10 mRNA. The Myo10 MO was microinjected into two cell embryos, and Western blot analysis of lysates made from embryos 24 h after injection showed that Myo10 protein levels were sharply reduced in Myo10 MO-injected embryos (morphants) compared with uninjected controls (Fig. 2 a).

Controls and Myo10 morphants were fixed and stained for α-tubulin at 12, 16, and 24 h after microinjection, and mitotic spindles in the outermost epithelial layer of the embryo were assessed for defects. At 12 h, no discernible mitotic phenotype was seen; however, by 16 h, Myo10 morphants showed a clear multipolar spindle phenotype, which was further enhanced by 24 h (Fig. 2, b and c). At 24 h, an increase in the number of normal bipolar spindles was also seen in the morphants compared with water-injected controls (Fig. 2 c). The increase in bipolar spindles in morphants likely reflects a delay in mitotic progression (see following section). Further analysis of the morphant spindles revealed a third spindle phenotype; Myo10 morphant spindles were significantly longer than controls, both in terms of absolute length (not depicted) and when corrected for cell size (Fig. 2 d). To test if other aspects of spindle organization were affected in morphants, propidium iodide was used to visualize chromosomes. As in controls, most of the chromosomes were localized near to the metaphase plate in morphant metaphase spindles (Fig. 2 e). Moreover, Myo10 morphant spindles in the early stages of the phenotype, exhibiting increased length and one or two extra poles, were observed to have similar chromosomal content to controls (Fig. 2 e), which indicates that these phenotypes were not an indirect result of a previous failed cell division.

To ensure that these phenotypes represent Myo10 depletion, two control experiments were performed: the morphant phenotype was rescued by microinjection of full-length Myo10 (see "The head and tail of Myo10…" and Fig. 5), and embryos were microinjected with a mispair control MO. The control MO differed from the Myo10 MO by just five mispairing nucleotides, and gave a reduced level of Myo10 knockdown (Fig. 2 a) and a correspondingly reduced level of phenotype compared with the morphant (Fig. 2 c), which indicates that Myo10 is the relevant target of the MO. Although these controls demonstrated the specificity of the MO, it was possible that knockdown of Myo10 in the embryo caused spindle defects indirectly by, for example, disrupting nuclear architecture or previous cytokinetic events. To test if the effect on spindle structure was direct, we used the *X. laevis* egg extract system to assemble spindles in vitro in the absence or presence of a Myo10 antibody. Although control spindles displayed normal bipolar morphology, spindles assembled in the presence of the Myo10 antibody appeared longer and exhibited multipolar phenotypes similar to those in the Myo10 morphants (Figs. 2 f and S2, available at http://www.jcb.org/cgi/content/full/jcb.200804062/DC1).

Myo10 morphant spindles are initially bipolar and then undergo pole fragmentation

The fact that chromosomes localized near the metaphase plate in Myo10 morphant spindles suggested that these spindles initially assembled normally. To explore this possibility, live confocal imaging was used. Using GFP–α-tubulin to visualize

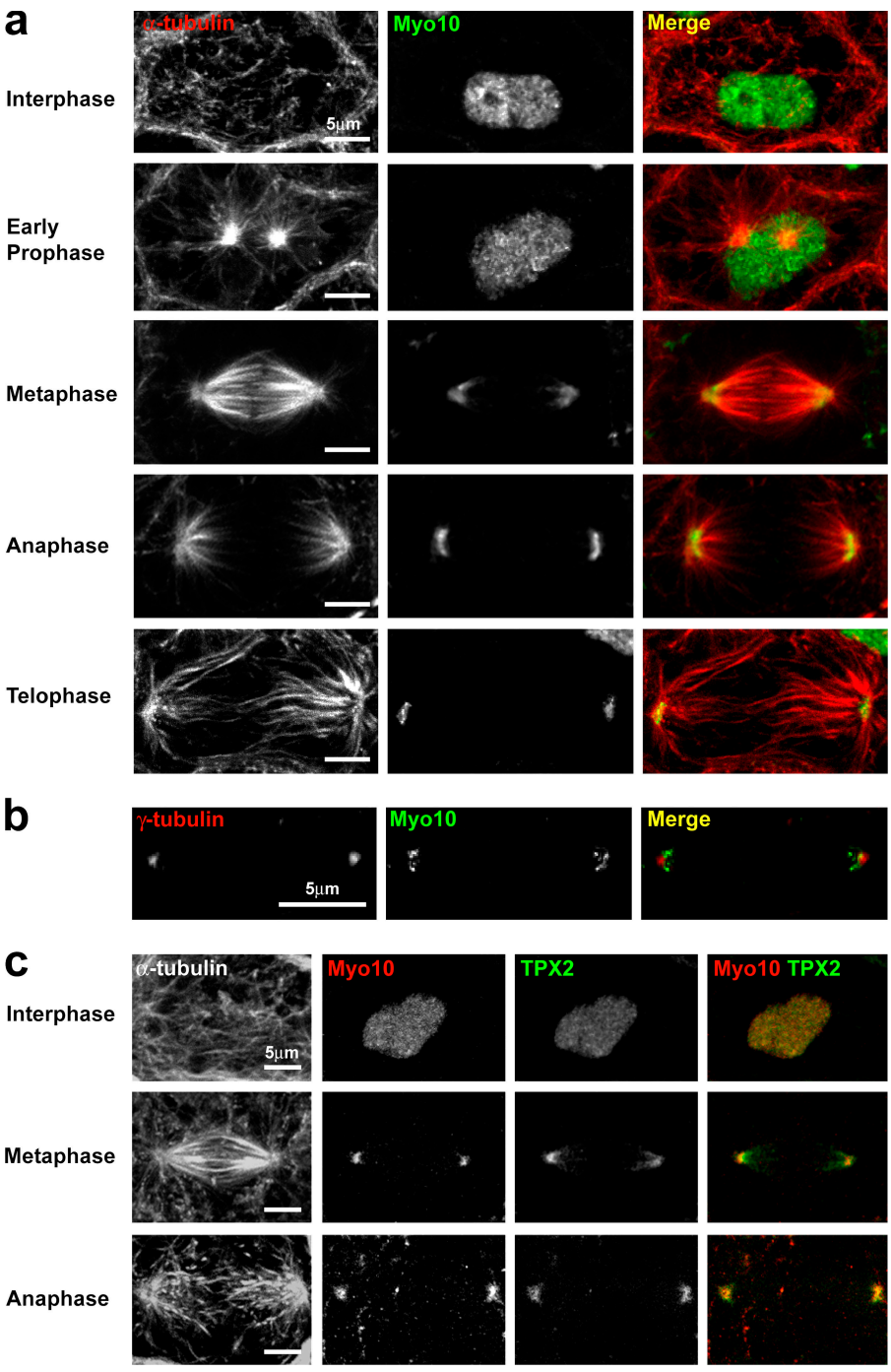

Figure 1. **Myo10 localizes to mitotic spindle poles in *X. laevis* embryos.** (a) Confocal micrographs of interphase and mitotic cells in the epithelium of *X. laevis* embryos double stained for α-tubulin (red) and Myo10 (green). During interphase and prophase, Myo10 localizes to the nucleus. From metaphase, Myo10 can be seen localized as a band close to the pole, a position it maintains through anaphase and telophase. Throughout the cell cycle, Myo10 is also found at the cell cortex (see Fig. S1, available at http://www.jcb.org/cgi/content/full/jcb.200804062/DC1) but is less obvious in these images, as fluorescent levels were reduced due to the high intensity of the nuclear staining. (b) Confocal images of an anaphase spindle double stained for γ-tubulin (red) and Myo10 (green) showing that Myo10 localizes to a region just inside the spindle pole marker γ-tubulin. (c) Confocal micrographs of spindles immunostained for α-tubulin, Myo10 (red), and TPX2 (green) showing that Myo10 and TPX2 display significant colocalization.

mitotic spindles, we found that it was possible to follow mitosis live in the cells of *X. laevis* embryonic epithelium by time-lapse confocal microscopy (Fig. 3 a and Video 1, available at http://www.jcb.org/cgi/content/full/jcb.200804062/DC1). Live imaging revealed four features of the Myo10 morphant phenotype that were not apparent from fixed cell analysis. First, in the initial stages of the morphant phenotype, spindles assembled normally with two poles, although these spindles were longer than controls (Videos 2 and 3). Second, supernumerary poles formed via fragmentation of the original poles, and rather than a wholesale fragmentation, fragmentation was quantal, with only one supernumerary pole forming from each original pole at a time (Fig. 3 b and Videos 2–4). Third, morphant spindles delayed in metaphase for significant periods of time: morphant metaphase took a mean 46.0 ± 8.0 min (n = 5), with 25.4 ± 3.2 min of that time spent as a bipolar spindle, before any pole fragmentation, compared with a metaphase duration of 6.6 ± 0.5 min (n = 4) in controls. The morphant metaphase delay could explain the increase in bipolar spindles seen in the fixed analysis of the morphant (Fig. 2, b and c). Fourth, as the morphant phenotype progressed, cytokinesis failures began to manifest, both in cells where spindles were elongated but remained bipolar (Video 5) and also in those where multipolar spindles, after a long delay, entered

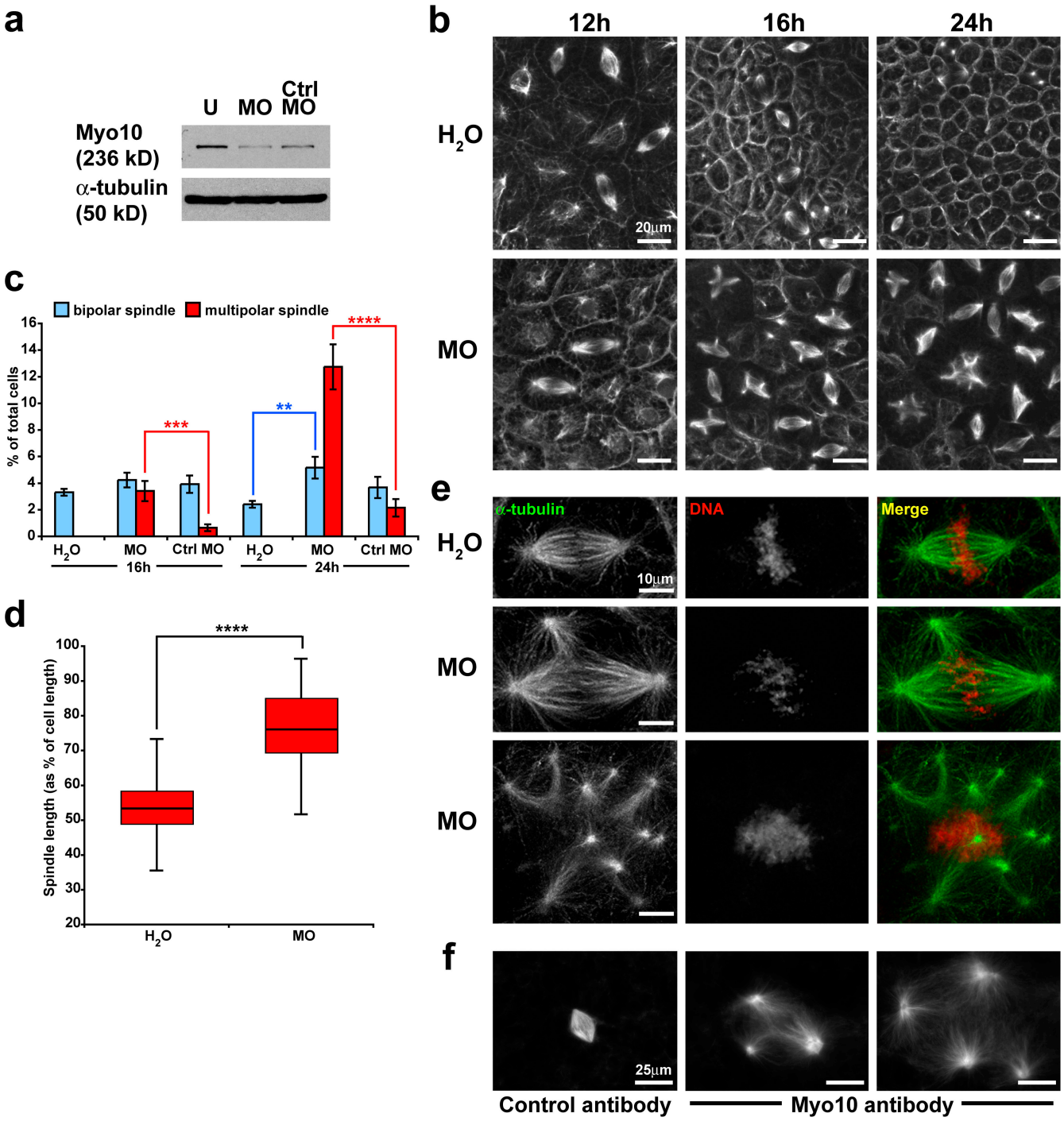

Figure 2. **Knockdown of Myo10 leads to mitotic spindle defects.** (a) Western blot showing Myo10 protein levels in uninjected (U), Myo10 MO (MO), and 5-mispair control MO (Ctrl MO) embryos. Lysates were prepared from embryos 24 h after microinjection. (b) Confocal micrographs of α-tubulin staining in embryos microinjected with nuclease-free water or Myo10 MO (MO) fixed at 12, 16, or 24 h after microinjection. (c) Quantification of mitotic spindles in water (H_2O)-, Myo10 MO (MO)-, and 5-mispair control MO (Ctrl MO)-injected embryos 16 and 24 h after microinjection. At 16 and 24 h, Myo10 morphants have significantly more multipolar spindles than the mispair control (red). An increased number of bipolar spindles is seen in the morphant at 24 h, which is suggestive of a delay in mitosis (n = 15, 11, 14, 17, 18, and 18 embryos for water 16 h, MO 16 h, Ctrl MO 16 h, water 24 h, MO 24 h, and Ctrl MO 24 h, respectively). Error bars represent the standard error of the mean. (d) Box and whisker plots displaying metaphase spindle length in water (n = 92 spindles)- and Myo10 MO (n = 50 spindles)-injected embryos 24 h after injection. Spindle length measurements are shown as a percentage of total cell length to control for differences in cell size. Metaphase spindles in the Myo10 morphant are significantly longer than in water-injected controls. (e) Propidium iodide (red) and α-tubulin (green) staining of control and morphant spindles showing that chromosomes localize to the metaphase plate relatively normally in morphant spindles. (f) Confocal micrographs of α-tubulin–stained spindles assembled in vitro in the presence of either a control antibody or an anti-Myo10 antibody. In control conditions, normal bipolar spindles assemble, whereas the inhibition of Myo10 by antibody addition leads to multipolar spindles. For significance testing, unpaired Student's t tests were performed: **, $P < 0.01$; ***, $P < 0.001$; ****, $P < 0.0001$.

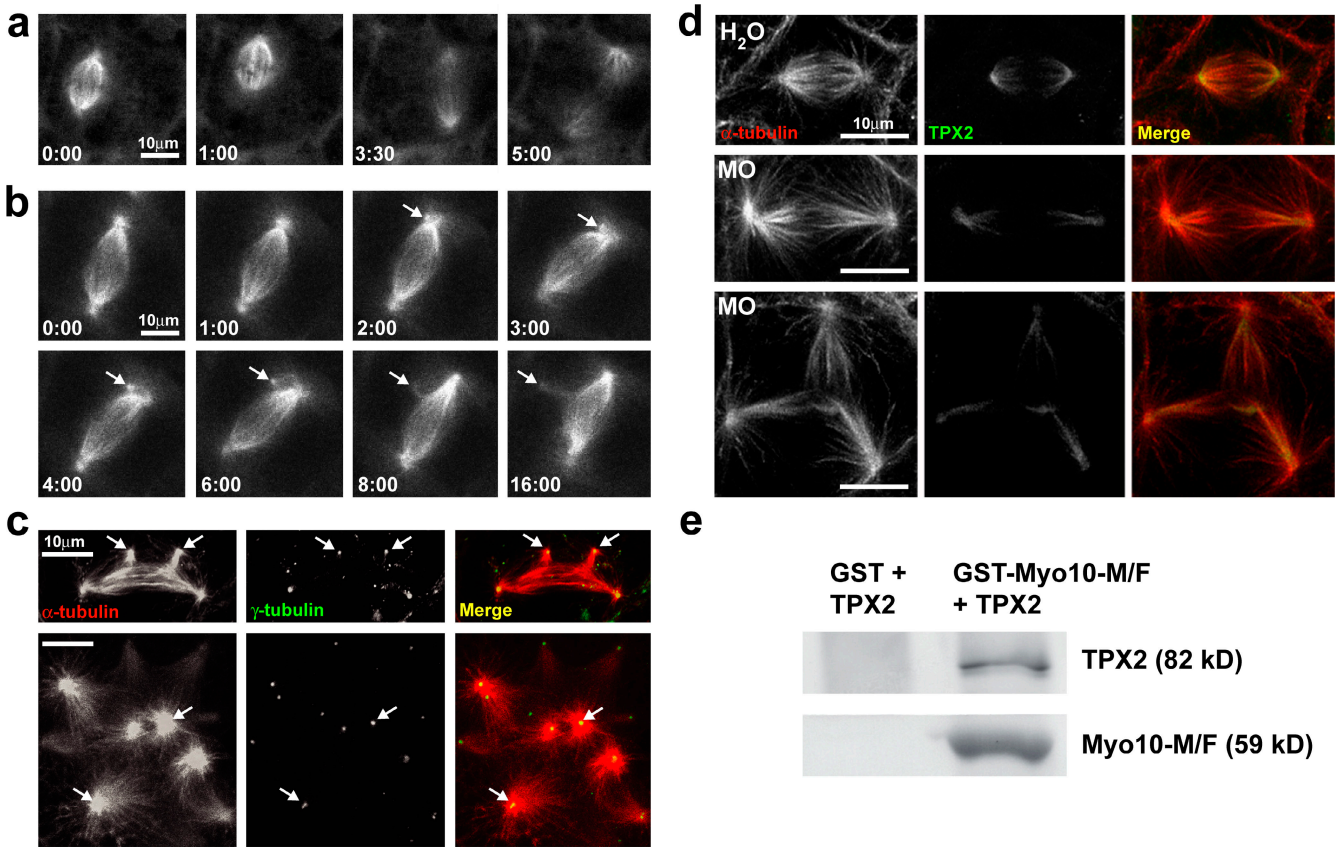

Figure 3. **Mitotic spindles in Myo10 morphants undergo spindle pole fragmentation, and Myo10 interacts with the spindle assembly factor TPX2.** (a) Stills taken from a confocal video (Video 1, available at http://www.jcb.org/cgi/content/full/jcb.200804062/DC1) of mitosis in a control embryo using GFP–α-tubulin to visualize the spindle; time stamps indicate time in minutes and seconds. (b) Stills taken from a video of a Myo10 morphant spindle (Video 4) showing that it assembles in a bipolar fashion, but, subsequently, a pole fragments to form a supernumerary pole (arrows). (c) Confocal micrographs of mitotic spindles in Myo10 morphants immunostained for α-tubulin (red) and γ-tubulin (green). All supernumerary poles in the multipolar spindles possess γ-tubulin, independent of whether the poles have just arisen (top, arrows) or are more established (bottom, arrows). (d) Mitotic spindles in water-injected and Myo10 morphant embryos immunostained for α-tubulin (red) and TPX2 (green). TPX2 localization is diffuse in the Myo10 morphant compared with the more focused pole localization in controls. (e) Western blot of GST pull-down assay showing that full-length TPX2 pulls down with GST-Myo10-MyTH4/FERM (GST-Myo10-M/F) but not GST alone.

a disorganized anaphase and attempted cytokinesis (Video 2). As a result of these aberrant divisions, binucleate cells were often seen at later time points, and when these cells entered mitosis, spindles were multipolar from the onset of assembly (Videos 2 and 6).

To gain more insight into the multipolar aspect of the Myo10 morphant phenotype, further immunostaining of the spindles was performed. The spindle pole marker γ-tubulin localized to every supernumerary pole in morphant multipolar spindles, irrespective of whether the spindle had recently undergone pole fragmentation (in spindles with one or two extra poles; Fig. 3 c) or was a more established multipolar spindle (three or more extra poles; Fig. 3 c). Morphant spindles were also stained to assess the localization of the spindle assembly factor TPX2. Intriguingly, TPX2 localization was more diffuse in morphant spindles compared with controls, with TPX2 no longer showing a strong concentration at the spindle pole but instead spreading down the spindle microtubules toward the metaphase plate (Fig. 3 d). This result indicated that Myo10 might be required to recruit or maintain TPX2 at the spindle pole during mitosis. To test for an interaction between Myo10 and TPX2, a GST pull-down assay was performed using the MyTH4/FERM domain cassette of Myo10 and full-length TPX2. This assay demonstrated that Myo10 binds directly to TPX2 via its MyTH4/FERM cassette (Fig. 3 e).

Abnormal spindle movement and anchoring in Myo10 morphants

Mitotic spindles in control embryos typically underwent a great deal of abrupt movement in the cell during metaphase, such that they rotated with a jerky motion, dramatically changing their position in very short periods of time (Fig. 4 a and Video 1). In contrast, Myo10 morphant spindles, even before they sprouted supernumerary poles, rotated with a much smoother motion (Fig. 4 b and Videos 2 and 3). Rotation rate measurements showed that control spindles underwent only slight rotation before metaphase, displayed the greatest changes in rotation rate during metaphase, and rotated slower once anaphase began (Fig. 4 c, blue). In comparison, morphant spindles never reached the same extremes in rotation rate but instead gently rotated throughout their extended metaphase; similar movement continued after spindle pole fragmentation and remained unchanged right up to an aberrant anaphase (Fig. 4 c, red).

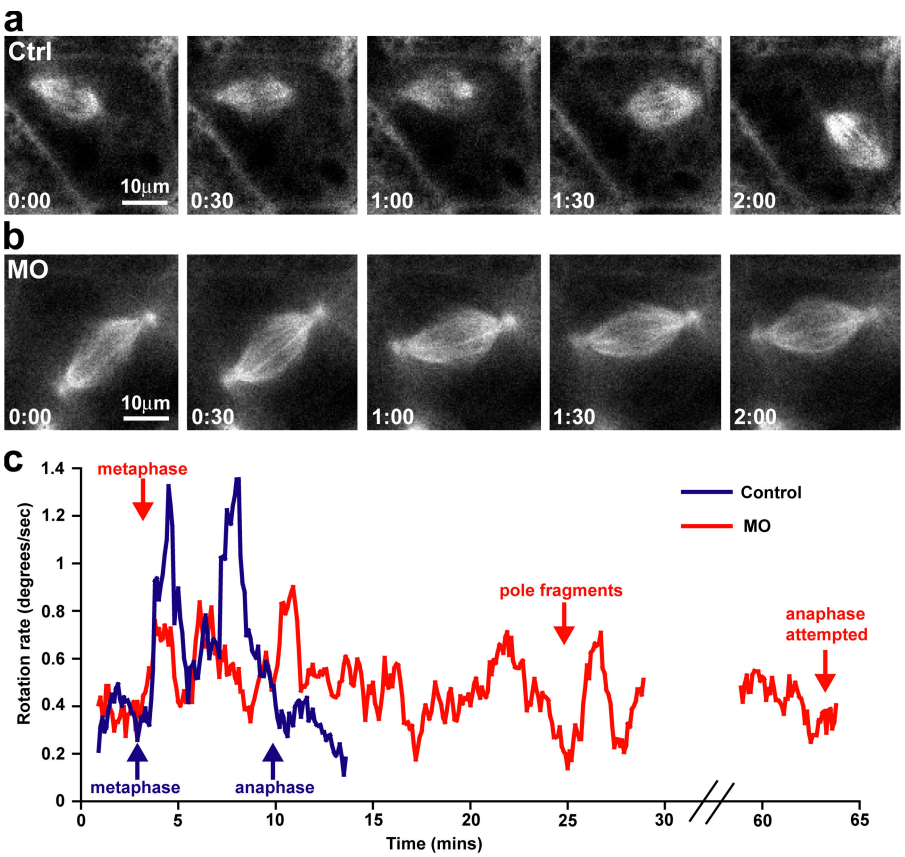

Figure 4. **Spindle movement is attenuated in Myo10 morphants.** (a) Stills taken from a short section of a confocal movie of GFP–α-tubulin in a control embryo (Video 1, available at http://www.jcb.org/cgi/content/full/jcb.200804062/DC1). Time stamps indicate time in minutes and seconds. The metaphase spindle undergoes a sudden movement between t = 1:00 and t = 2:00; this "jerky" rotational movement is characteristic of metaphase spindles in control embryos at embryonic stages 9 and 10. (b) Stills taken from confocal movie of GFP–α-tubulin in a Myo10 morphant (Video 2) at the same embryonic stage as the control embryo in panel a. The morphant spindle, even while still bipolar, displays a much more gradual rotational movement than the control spindle. (c) A graph displaying the rotational movement of a control spindle compared with a Myo10 morphant spindle. The time at which spindles enter metaphase and anaphase or undergo pole fragmentation are indicated by arrows and accompanying labels.

The head and tail of Myo10 have distinct mitotic roles

The N-terminal head domain of Myo10 binds to F-actin (Homma et al., 2001), whereas the C-terminal tail contains a MyTH4/FERM domain cassette that binds microtubules (Weber et al., 2004). To determine if the different mitotic functions of Myo10 were mediated through different regions of the myosin, rescue experiments were performed (see Fig. 5 a for schematics of rescue constructs). Microinjection of full-length Myo10 (GFP-Myo10) into morphants gave a strong rescue of the key mitotic phenotypes: GFP-Myo10 reduced the increased number of bipolar spindles seen in the morphant (Fig. 5, b and c), reduced spindle pole fragmentation (Fig. 5, b and c), and reduced spindle length (Fig. 5 d). In contrast the GFP–Myo10–heavy meromyosin (HMM) construct, an HMM-like fragment that contains the myosin motor, regulatory IQ domains, and coiled coil domains of Myo10, reduced the number of bipolar spindles (Fig. 5 c) and shortened spindle length (Fig. 5 d) but did not rescue the multipolar phenotype (Fig. 5 c). Remarkably, the GFP-Myo10-IQT construct, which lacks the motor domain but contains the tail, IQ, and coiled coil domains, gave the opposite result: the multipolar phenotype was significantly rescued but bipolar spindle numbers were not reduced (Fig. 5 c) and the spindle length phenotype was only partially rescued (Fig. 5 d). These results indicated that the actin-binding head was required for proper progression through mitosis and for maintaining spindle length, two functions that may be linked, whereas the microtubule-binding tail was required for spindle pole integrity.

F-actin and Myo10 function antagonistically to maintain spindle length

The involvement of an actin-based motor in mitosis led us to consider whether actin might be required for mitotic spindle functions. To explore this possibility, morphant and water-injected embryos were treated with low concentrations of latrunculin B (LatB) for 30 min to disrupt F-actin and then immediately fixed and stained for α-tubulin. Treatment of water-injected embryos with LatB caused cells of the epithelium to round up but did not increase the number of bipolar spindles, promote spindle pole fragmentation, or significantly affect mean spindle length (Fig. 6, a, c, and d). However, LatB treatment resulted in impaired anchoring such that spindles oriented perpendicular to the plane of the epithelium, unlike the parallel arrangement in controls (Fig. 6 a). Treatment of Myo10 morphant embryos with LatB had no significant effect on the number of bipolar or multipolar spindles (Fig. 6 c). However, a startling affect on spindle length was seen when Myo10 morphants were treated with LatB: the longer spindles seen in the morphant were rescued by disrupting F-actin (Fig. 6, b and d), which suggests that Myo10 and F-actin function antagonistically to maintain spindle length.

Live imaging reveals actin cables in and around the mitotic spindle

The role and distribution of F-actin in the mitotic spindle has long been controversial (see Introduction), but the finding that F-actin and Myo10 together played a role in controlling spindle length prompted us to reinvestigate F-actin distribution in mitotic cells. To visualize F-actin in living embryos, we used a recently

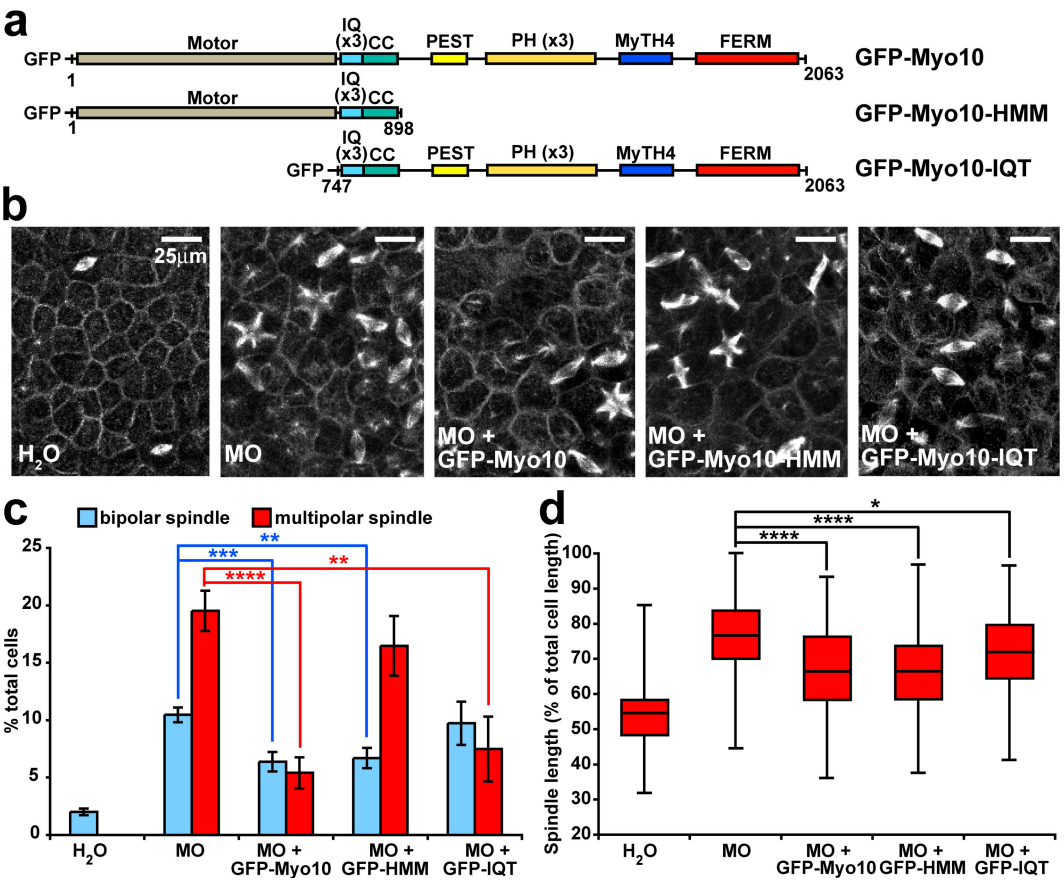

Figure 5. **Rescue experiments reveal that the head and tail of Myo10 mediate different aspects of Myo10 function in mitosis.** (a) Schematic diagram of the constructs used in Myo10 morphant rescue experiments. (b) Low-magnification images of α-tubulin staining in rescue experiment embryos. For these experiments, embryos were microinjected with water or Myo10 MO along with RNA encoding each of the Myo10 constructs shown in panel a. (c) Quantification of bipolar and multipolar spindles in rescue experiment embryos. *n* = 18, 47, 22, 16, and 12 embryos for water, MO, MO + GFP-Myo10, MO + GFP-Myo10-HMM, and MO + GFP-Myo10-IQT, respectively. Error bars represent the standard error of the mean. (d) Box and whisker plots of spindle length measurements in rescue experiment samples. Spindle length was calculated as a percentage of total cell length to allow for variation in cell size. *n* = 109, 141, 136, 115, and 87 spindles for water, MO, MO + GFP-Myo10, MO + GFP-Myo10-HMM, and MO + GFP-Myo10-IQT, respectively. For significance testing, unpaired Student's *t* tests were performed: *, P < 0.05; **, P < 0.01; ***, P < 0.001; ****, P < 0.0001.

developed probe consisting of GFP fused to the calponin homology domain of utrophin (GFP-Utr-CH), which labels F-actin with low background and no apparent effect on F-actin dynamics (Burkel et al., 2007). Live imaging of embryos microinjected with GFP-Utr-CH and mCherry–α-tubulin revealed that F-actin was present in control mitotic spindles. Dynamic actin cables were seen surrounding and running the length of the spindle as it assembled, and these cables remained associated with the spindle through early mitosis (Fig. 7 a, arrows; and Video 7, available at http://www.jcb.org/cgi/content/full/jcb.200804062/DC1). Many F-actin cables were also concentrated around the spindle poles, with some cables extending between the poles and the cell cortex (Fig. 7 b and Video 7). As spindles rotated during metaphase, the arrangement of F-actin cables mirrored this movement, as if the cables helped to determine the direction of spindle motion (Fig. 7 c and Video 8). As spindles entered anaphase, F-actin remained concentrated around the poles (Fig. 7 a and Video 8).

A previous study indicated that Myo10 has the ability to organize F-actin (Tokuo et al., 2007), and to explore this possibility, we imaged F-actin live in Myo10 morphants. However, we saw no obvious change in cortical or spindle-associated F-actin in the Myo10 morphants, although it is possible that there are subtle changes to F-actin organization that are beyond the sensitivity of our current imaging methods. In particular, F-actin cables could still be seen surrounding the morphant spindle as it assembled, just as was observed in controls (Fig. 7 d and Video 9, available at http://www.jcb.org/cgi/content/full/jcb.200804062/DC1). In multipolar morphant spindles, F-actin was concentrated around all the poles, including supernumerary poles, and tracked with the movement of the spindle (Fig. 7 e and Video 9).

Discussion

In this study, we show that Myo10 localizes to the mitotic spindle pole and plays several important roles in mitosis: spindle anchoring, maintenance of spindle pole integrity, spindle length control, and mitotic progression. Surprisingly, the relationship between Myo10 and F-actin varies depending on the role in question, with Myo10 and F-actin playing similar roles in spindle anchoring/positioning, Myo10 functioning independently of F-actin to maintain spindle pole integrity, and Myo10 and F-actin working antagonistically to control spindle length.

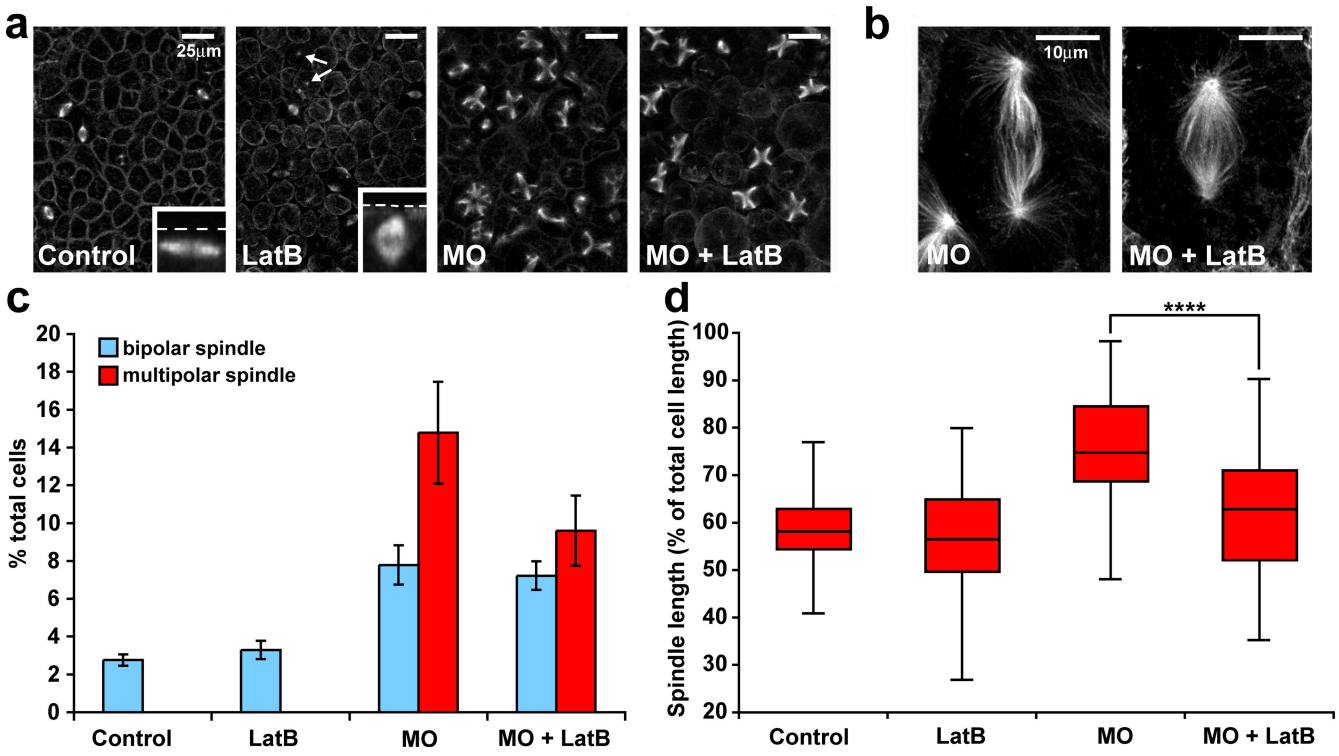

Figure 6. **Depolymerizing F-actin rescues spindle length but not multipolarity in Myo10 morphants.** (a) Low-magnification confocal micrographs of mitotic spindles in untreated embryos (control and MO) or embryos incubated in 2.5 μM LatB (MO + LatB). In LatB-treated embryos, some spindles were improperly oriented perpendicular to the plane of the epithelium (arrows). Insets show z projection cross sections of a control spindle, oriented parallel to the plane of the epithelium, and a LatB spindle in the improper perpendicular orientation (the outermost cell cortex is indicated by a broken line in each inset). (b) High-magnification confocal micrographs of α-tubulin–stained spindles in Myo10 morphants either untreated (MO) or incubated in 2.5 μM LatB (MO + LatB). (c) Quantification of spindles in LatB experiment embryos shows that treatment with LatB does not significantly affect the number of bipolar or multipolar spindles (n = 11, 11, 17, and 15 embryos for control, LatB, MO, and MO + LatB, respectively). Error bars represent standard error of the mean. (d) Box and whisker plots of spindle length measurements in the LatB experiment; spindle length was calculated as a percentage of total cell length to allow for changes in cell size. Treatment with LatB significantly rescues the increased spindle length seen in Myo10 morphants (n = 82, 104, 86, and 59 spindles for control, LatB, MO, and MO + LatB, respectively). For significance testing, unpaired Student's t tests were performed: ****, $P < 0.0001$.

Our findings indicate that Myo10 and F-actin both help to anchor the spindle during mitosis. First, spindles in Myo10 morphants undergo strikingly different movements to controls, with morphant spindles moving smoothly compared with the rapid changes in rotation rate displayed by control metaphase spindles. Second, disrupting F-actin in embryos leads to spindle positioning defects, with spindles orienting perpendicular, rather than parallel, to the cortex. The fact that knocking down Myo10 eliminates jerky spindle movement suggests that Myo10 functions in spindle anchoring by providing transient links between the spindle and the cortex through brief, high-affinity interactions with F-actin, generating a stop-start movement. It may seem counterintuitive that disrupting anchoring would lead to a reduction in rotation rate, but this phenomenon has also been seen in the *Caenorhabditis elegans* embryo, where knockdown of dynein, a microtubule motor that is located at the cell cortex and pulls on spindle microtubules, leads to an attenuation of spindle oscillation (Pecreaux et al., 2006). It is unclear whether Myo10's spindle anchoring capacity is mediated through cortically localized Myo10, possibly functioning in concert with cortical dynein, or through Myo10 associated with the spindle. However, it is interesting to note that because we see actin cables extending between the cortex and the spindle pole, the latter possibility is highly plausible. The notion that Myo10 acts to anchor the spindle through interactions with F-actin fits well with the fact that actin is known to play a vital role in positioning the spindle during oriented cell division (Gundersen and Bretscher, 2003; Rodriguez et al., 2003; Gundersen et al., 2004) and the recent finding that Myo10 is required for spindle orientation in cultured mammalian cells (Toyoshima and Nishida, 2007).

A second function of Myo10 during mitosis is to maintain spindle pole integrity, as disrupting Myo10 either in vitro or in vivo leads to the formation of multipolar spindles. An unusual aspect of this phenotype is that spindle poles first appear to assemble normally and only fragment subsequently. This suggests that Myo10 is not required to establish bipolarity during spindle assembly but instead acts to stabilize spindle poles as mitosis progresses, although it is also possible that the late onset of the multipolar phenotype simply reflects a slow loss of Myo10 protein in morphant cells. It is interesting to note that a similar late-onset pole fragmentation phenotype is seen when Borealin, a member of the chromosomal passenger complex, is depleted in mammalian cells (Gassmann et al., 2004). Exploring a link between Myo10 and this complex could be a fruitful area for further study. Strikingly, the function of Myo10 in the spindle pole is independent of F-actin, as LatB treatment has no effect on spindle pole integrity either in control or morphant embryos. Furthermore, injection

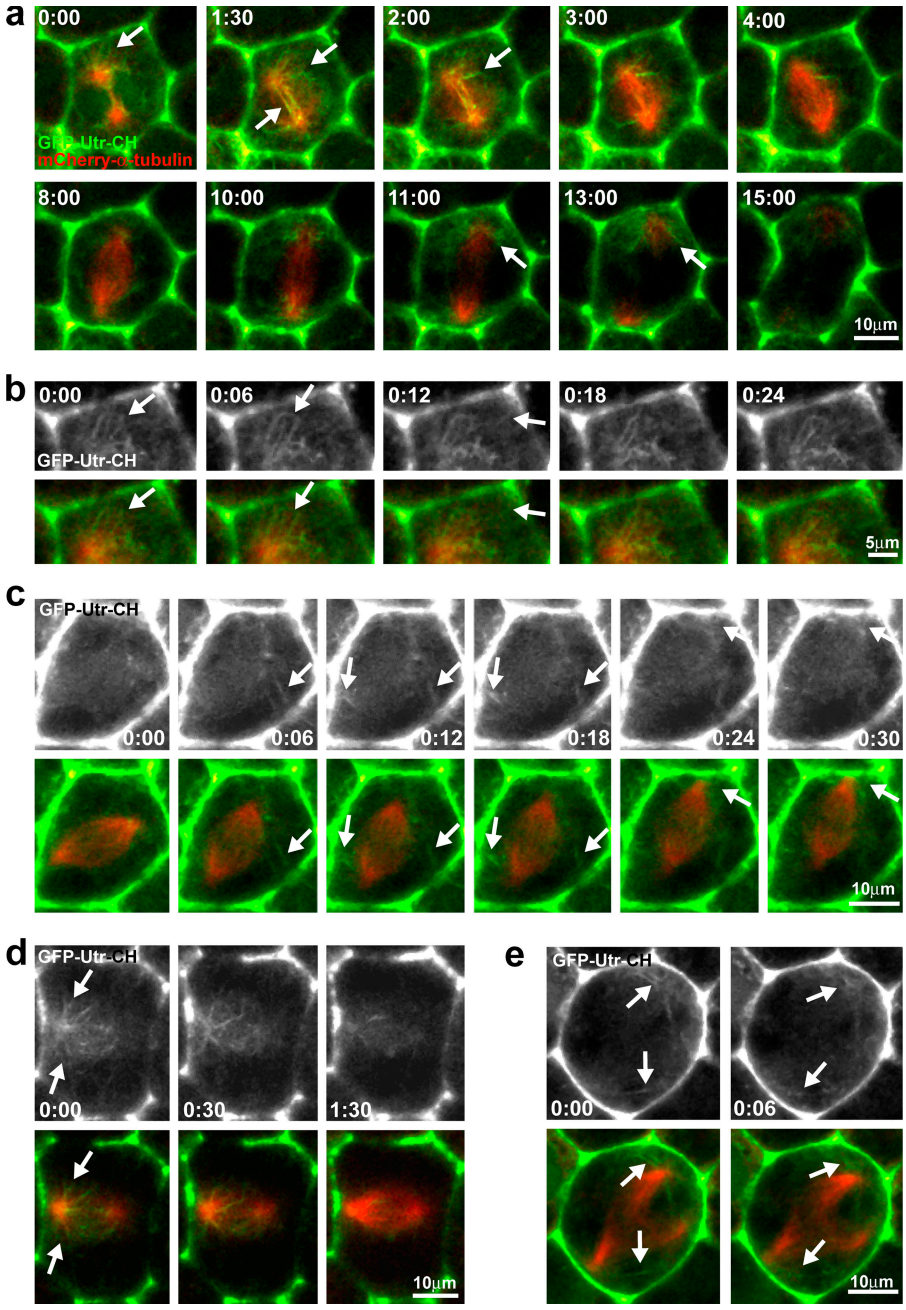

Figure 7. **Live imaging in *X. laevis* embryos reveals actin cables around the mitotic spindle, which are unaffected in Myo10 morphants.** (a) Images taken from a video showing F-actin organization in a control mitotic spindle (see Video 7, available at http://www.jcb.org/cgi/content/full/jcb.200804062/DC1) using mCherry–α-tubulin (red) to visualize the spindle and the GFP-Utr-CH probe (green) to visualize F-actin. Highly dynamic F-actin cables surround the spindle as it assembles (t = 0:00–2:00, arrows) and are concentrated around the poles later in mitosis, especially during anaphase (t = 11:00 and 13:00, arrows). (b) An enlarged view of the uppermost spindle pole from panel a showing that F-actin (GFP-Utr-CH, green) is concentrated around the pole, with some F-actin cables appearing to emanate from the pole (t = 0:00 and 0:06, arrows) and others from the cortex (t = 0:12, arrows). (c) Stills taken from a video of a second control spindle (see Video 8) demonstrating that the assembly of F-actin cables between the spindle and the cell cortex coincide with spindle movement (t = 0:00–0:18, arrows) and concentrate as a pole is drawn toward the cortex (t = 0:24 and 0:30, arrows). (d) Images taken from a video showing F-actin (GFP-Utr-CH, green) organization during Myo10 morphant spindle assembly (see Video 9). F-actin cables associate with the morphant spindle as it assembles (arrow), just as occurs in controls. (e) Stills of a multipolar spindle in a Myo10 morphant (see Video 9) demonstrating that F-actin associates with each of the poles and follows the motion of the spindle (arrows). In each panel, time stamps indicate time in minutes and seconds.

of GFP-Myo10-IQT, a Myo10 tail construct that lacks the actin-binding myosin head, specifically rescues the pole fragmentation phenotype in Myo10 morphants. A possible explanation for Myo10 tail function in spindle pole integrity is that domains in the tail act to recruit and/or retain pole proteins such as TPX2, NuMA, or γ-tubulin at the pole. Consistent with this idea, disruption of TPX2 has been previously shown to generate multipolar spindles (Garrett et al., 2002), and we find that TPX2 fails to localize properly to the spindle pole in Myo10 morphants. In addition, Myo10 can interact directly with TPX2 via its MyTH4/FERM domain cassette. However, it remains unclear how TPX2 functions in spindle pole focusing, and our data do not rule out the possibility that TPX2 is instead required to recruit Myo10 to the pole to ensure pole integrity; resolving this issue will be an important line of further investigation. The upstream control of TPX2 is much better understood, as, like other spindle assembly factors, TPX2 is held at the nucleus during interphase through an interaction with the nuclear importins and is released from this by Ran GTPase as mitosis begins (Gruss and Vernos, 2004). It is interesting to note the similarities between the localization patterns of Myo10 and TPX2 and consider if Myo10 localization may also be regulated by the Ran GTPase pathway. Previous work has shown that the tail of Myo15, a MyTH4/FERM myosin, binds to the nuclear importin, importin-α (Liu et al., 2008), and, intriguingly, we also find by yeast two-hybrid assay that the MyTH4/FERM domain cassette of Myo10 interacts with importin-α (unpublished data), which suggests that the localization of Myo10 may be controlled in a similar manner to spindle assembly factors.

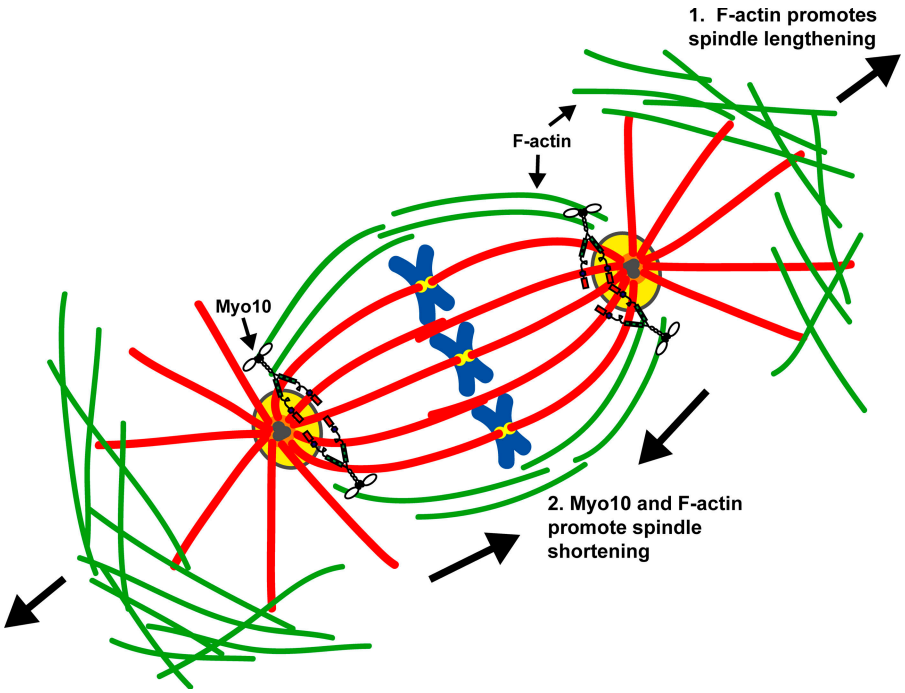

Figure 8. **Model for spindle length regulation by F-actin and Myo10.** F-actin and Myo10 function antagonistically to contribute to spindle length control. F-actin promotes spindle lengthening, perhaps through interactions with astral microtubules at the cell cortex, whereas Myo10 provides a counteracting spindle shortening function. The F-actin spindle lengthening is independent of Myo10, as knockdown of Myo10 results in longer spindles. In contrast, the shortening function of Myo10 requires F-actin because disrupting both F-actin and Myo10 gives normal length spindles.

A third role for Myo10 in mitosis is regulation of spindle length. Specifically, Myo10 depletion results in spindles that are significantly longer than controls, both in absolute terms and as a function of cell size. Remarkably, this increased spindle length is rescued by disruption of F-actin with LatB, indicating that Myo10 and F-actin somehow play opposing roles in mitotic spindle length control. How can these findings be reconciled? The simplest explanation is that actin filaments participate in mutually opposing mechanisms that control spindle length: one mechanism that lengthens spindles and is independent of Myo10 and one that shortens spindles and is dependent on Myo10 (Fig. 8). When Myo10 is depleted, the former predominates, causing spindle lengthening; when F-actin is disrupted by latrunculin treatment either with or without Myo10 depletion, both mechanisms are neutralized, so spindle lengths are similar to controls. This model is attractive not only because it explains the results of the current study, but also because it might account for previous findings in *X. laevis* egg extracts showing that F-actin disruption has no obvious effect on spindle length (Mitchison et al., 2005). Curiously, in the current study, addition of Myo10 antibodies to extracts resulted in spindles that appeared longer than controls, in spite of the fact that cytochalasin D was present. Although this might simply reflect the apparent fragmentation of the poles, there is another potential explanation. That is, previously, we have shown that microtubules in extracts interact with dynein immobilized on the glass substrate (Waterman-Storer et al., 2000), and it may be that this interaction produces an outward pulling force in the extract spindles, which is exaggerated when Myo10 is depleted.

Assuming one or more aspects of the above model are correct, it will be essential in future studies to determine how exactly the F-actin–dependent lengthening and shortening mechanisms work. Two general, nonexclusive possibilities should be considered. First, it is possible that the mechanisms work in a relatively direct manner, with the lengthening mechanism being underpinned by pulling forces on the poles via F-actin and dynein (Sharp et al., 2000) and/or myosin-2 (Rosenblatt et al., 2004), whereas the poles are pulled together by Myo10 acting on the spindle-associated F-actin described here. Alternatively, as considerable evidence links spindle length control to tubulin turnover within the spindle (Goshima et al., 2005; Mitchison et al., 2005), it is also possible that the F-actin–dependent spindle length control mechanisms function more indirectly, by modulating microtubule assembly and disassembly within the spindle. The F-actin cables that we see associated with the mitotic spindle could contribute to either of these mechanisms, and this will be an important area for further investigation.

The extent to which the various Myo10 roles described above are interrelated must be considered. The differential dependence on F-actin indicates that at least some aspects of the phenotypes can be considered separately. However, it is also likely that some of them are coupled. For example, it seems plausible that the metaphase delay is related to the spindle length defect, in that it is not hard to imagine that improper length control, and any subsequent loss of tension, would elicit the spindle assembly checkpoint (Nicklas et al., 1995; Zhou et al., 2002). Further, it is also probable that at least some of the deficits that result from Myo10 depletion feed back on each other. That is, in videos where the phenotype is just starting to become manifest, excessive spindle length and metaphase delay are apparent before excessive spindle pole fragmentation (e.g., Video 2). However, at least some of the cells with elongate spindles fail to complete cytokinesis without having obviously fragmented their poles (e.g., Video 5). Such cells would thus start the subsequent mitosis with additional poles. This condition would, presumably, further delay metaphase, provide additional material for pole fragmentation, and increase the probability of another failed cytokinesis. Consequently, in just one or two cell cycles, cells could go from an

initially modest phenotype, wherein spindles have just two extra poles, to the severe phenotype in which upwards of 15 extra poles are apparent (e.g., Fig. 2, b and e).

Materials and methods

Egg procurement and in vitro fertilization
Adult *X. laevis* females were first primed for ovulation by injection with 50 units of human chorionic gonadotrophin (HCG; MP Biomedicals) into the dorsal lymph sac 4–7 d before use and then injected with an additional 800 units of HCG 18 h before use. Eggs were laid into 1× MMR (100 mM NaCl, 2 mM KCl, 1 mM $MgCl_2$, and 5 mM Hepes, pH 7.4) and fertilized by adding macerated testes. 30 min after fertilization, embryos were dejellied in 2% cysteine (in 1× MMR, pH 7.8) and rinsed five times with 1× MMR and five times with 0.1× MMR. Embryos were cultured in 0.1× MMR at 17°C.

Embryo microinjection
RNA for microinjection was made as described previously using pCS2-EGFP, pCS2-mCherry, or pStain vectors (Sokac et al., 2003). Microinjections were delivered using a PLI-100 picoinjector (Medical Systems), with embryos submerged in 0.1× MMR + 5% Ficoll. Myo10 MO (MO sequence: 5′-TATTCCTCCATGTCTCCCTCTGCTC-3′; Gene Tools, LLC) or 5-mispair control MO (5′-TATTCgTCgATcTCTCgCTCTcCTC-3′, lowercase letters indicate mispairing nucleotides) were heated for 5 min at 65°C before microinjection and microinjected into two- or four-cell embryos at a needle concentration of 0.5–1 mM. For live imaging of mitotic spindles, both cells of two-cell embryos were microinjected with 5 nl of RNA for EGFP–α-tubulin (needle concentration of 0.5 mg/ml) or mCherry–α-tubulin (0.5 mg/ml) and EGFP-Utr-CH (0.125 mg/ml), and embryos were subsequently microinjected at the four-cell stage in all cells with 2.5 nl of Myo10 MO (0.5 mM) or nuclease-free water. For morphant rescue experiments, both cells of two-cell embryos were microinjected with 5 nl of RNA for the GFP-tagged Myo10 constructs (0.5 mg/ml) and then subsequently microinjected at the four-cell stage with 2.5 nl of Myo10 MO (0.5 mM) or nuclease-free water. After microinjection, embryos were incubated at 17°C for 12–24 h in 0.1× MMR before processing for live imaging, fixation, or Western blot analysis.

In vitro spindle assembly
Cytostatic factor (CSF)-arrested *X. laevis* egg extracts were prepared as described previously (Murray, 1991). *X. laevis* sperm chromatin was added and the extracts were subsequently cycled into interphase by the addition of 400 μM Ca^{2+}. After 60 min, an equal volume of mitotic extract supplemented with Δ90 cyclin B (1:20) was added to induce spindle assembly. Samples were fixed 45 min after extract addition, spun onto coverslips, subsequently processed for immunofluorescence with the Myo10 antibody (1:100), and visualized, all as described previously (O'Brien et al., 2005). For Myo10 antibody addition experiments, Myo10 antibody (1:10) or a nonspecific rabbit IgG (1:20) was added just before mitotic extract addition.

Immunofluorescence
For immunofluorescent analysis of microtubules only, embryos were processed as described previously (Danilchik et al., 1998). For all other staining, the methanol postfix step was omitted from this protocol. Antibodies used were: anti–α-tubulin (DM1A; 1:200 dilution; Sigma-Aldrich), 5 μg/ml anti-Myo10 (Weber et al., 2004), anti-TPX2 (1:800; O'Brien and Wiese, 2006), mouse anti–γ-tubulin (GTU88; 1:200; Sigma-Aldrich), and 10 μg/ml rabbit anti–γ-tubulin (Keating and Borisy, 2000). To visualize chromosomes, embryos were first fixed and processed as above, omitting the methanol postfixation, and then permeabilized for 5 min at room temperature in PBS + 0.5% Triton X-100, equilibrated in 2× SSC (0.3 M $NaCl_2$ and 0.03 M sodium citrate, pH 7), treated with 100 μg/ml DNase-free RNase in 2× SSC for 20 min at 37°C, and then incubated with 5 μM propidium iodide (Invitrogen) in 2× SSC for 5 min at room temperature.

LatB treatment of embryos
Embryos were microinjected with nuclease-free water or Myo10 MO (needle concentration, 1 mM) into both cells at the two-cell stage and incubated at 17°C for 20 h. Embryos were then incubated for 30 min at room temperature in 0.1% DMSO or 2.5 μM LatB in 1× MMR. All embryos were fixed immediately after treatment and stained for α-tubulin as described in the previous paragraph.

Confocal imaging
For fixed tissue analysis, samples were mounted in Murray's Clear (benzyl benzoate/benzyl alcohol, 2:1) and imaged at room temperature using a microscope (Axiovert 100M ; Carl Zeiss, Inc.) with Lasersharp confocal software (Bio-Rad Laboratories) using 0.8 NA 25× or 1.4 NA 63× oil immersion objectives (Carl Zeiss, Inc.). Z series were acquired using step sizes of 0.25–1 μm and were reconstructed using Volocity software (PerkinElmer). For live imaging, embryos were mounted in 0.1× MMR (see "Egg procurement and in vitro fertilization") and imaged at room temperature using the Axiovert 100M microscope with a 1.4 NA 63× oil immersion objective. Single-plane time series were collected with intervals of 6 s and were processed using Volocity or ImageJ software.

Embryo lysates and immunoblotting
Embryo lysates were prepared from embryos microinjected with nuclease-free water, Myo10 MO (needle concentration, 1 mM), or 5-mispair control MO (1 mM), which had been incubated for 24 h after injection at 17°C. Embryos were homogenized in 7.5 μl of homogenization buffer (10 mM imidazol, 50 mM KCl, 2.5 mM $MgCl_2$, 1 mM EGTA, 2.5 mM ATP, 1 mM dithiothreitol, 10 mM EDTA, 0.5% Triton X-100, and protease inhibitors) per embryo on ice using a tight dounce homogenizer. Homogenized embryos were centrifuged briefly at 4°C to remove lipids and cell debris, and lysate supernatants were transferred to fresh Eppendorf tubes and boiled with 6× SDS sample buffer. Samples were then separated by 8% SDS-PAGE, transferred to nitrocellulose, and analyzed by Western blot according to standard protocols using 1 μg/ml anti-Myo10 and anti–α-tubulin (DM1A; 1:5,000 dilution; Sigma-Aldrich).

Protein expression and in vitro binding
GST-MyTH4-FERM was expressed in *Escherichia coli* strain C41(DE3) and purified on glutathione-agarose beads (Sigma-Aldrich) using standard protocols. TPX2 was purified and the tag was removed as described previously (O'Brien and Wiese, 2006). Purified proteins were concentrated to ∼5 mg/ml, dialyzed against a buffer containing 20 mM Tris-HCl, pH 7.5, 150 mM NaCl, and 1 mM DTT, flash frozen in small aliquots, and stored at −80°C. For the in vitro binding assay, ∼2 μM of each protein (GST-MyTH4-FERM, TPX2, or GST as indicated) in a total volume of 50 μl was incubated with 25 μl of glutathione-agarose beads at 4°C on a rotator for 1 h. The beads were retrieved by a brief spin, washed three times with H100 (O'Brien and Wiese, 2006), and eluted with 1× SDS sample buffer. Supernatants were brought to 1× with 4× SDS sample buffer. Samples were boiled and subsequently loaded and separated by 10% SDS-PAGE, transferred to nitrocellulose, and Western blotted according to standard protocols.

Quantification and statistical analysis
To quantify spindle phenotypes in embryos, the number of bipolar metaphase spindles, multipolar spindles, and total cells were counted in low magnification confocal micrographs of α-tubulin staining; >10 embryos were analyzed for each sample (*n* values are given in relevant figure legends). To determine mitotic spindle length in embryonic cells, two measurements were taken: pole-to-pole distance and total cell length, and spindle length was represented as a percentage of total cell length to allow for differences in cell size (>10 embryos and >50 spindles were analyzed for each sample). To test for a statistically significant difference between samples, unpaired Student's *t* tests were performed.

Online supplemental material
Fig. S1 shows cell cortex and spindle localization of Myo10. Fig. S2 shows quantification of spindles assembled in vitro in the presence of control or Myo10 antibody. Video 1 shows mitotic spindles in control embryonic epithelium. Video 2 shows mitotic spindles in Myo10 morphant epithelium. Video 3 shows mitotic spindles in Myo10 morphant epithelium. Video 4 shows spindle pole fragmentation in the Myo10 morphant. Video 5 shows failed cytokinesis in the Myo10 morphant. Video 6 shows multipolar spindle assembly in a binucleate cell in the Myo10 morphant. Video 7 shows that F-actin cables surround the mitotic spindle during assembly. Video 8 shows that F-actin cables extend between the cell cortex and the mitotic spindle during spindle rotation. Video 9 shows that F-actin organization is unaffected in Myo10 morphants. Online supplemental material is available at http://www.jcb.org/cgi/content/full/jcb.200804062/DC1.

Thanks to A.L. Miller, B.M. Burkel, and R.E. "Dick" Cheney for helpful advice, the organizers of the 2007 Gordon Research Conference on "Motile and Contractile Systems," which provided an extremely useful forum to discuss

these results, and B.A. Weaver and an anonymous reviewer for calling our attention to a very relevant paper.

This work was supported by a grant from the National Institutes of Health to W.M. Bement (GM52932-08), a grant from the National Science Foundation to C. Wiese (MCB-0344723) and a Predoctoral Fellowship from the University of Wisconsin-Madison Department of Biochemistry to L.L. O'Brien.

Submitted: 11 April 2008
Accepted: 6 June 2008

References

Barak, L.S., E.A. Nothnagel, E.F. DeMarco, and W.W. Webb. 1981. Differential staining of actin in metaphase spindles with 7-nitrobenz-2-oxa-1,3-diazole-phallacidin and fluorescent DNase: is actin involved in chromosomal movement? *Proc. Natl. Acad. Sci. USA.* 78:3034–3038.

Berg, J.S., and R.E. Cheney. 2002. Myosin-X is an unconventional myosin that undergoes intrafilopodial motility. *Nat. Cell Biol.* 4:246–250.

Berg, J.S., B.H. Derfler, C.M. Pennisi, D.P. Corey, and R.E. Cheney. 2000. Myosin-X, a novel myosin with pleckstrin homology domains, associates with regions of dynamic actin. *J. Cell Sci.* 113(Pt 19):3439–3451.

Burkel, B.M., G. von Dassow, and W.M. Bement. 2007. Versatile fluorescent probes for actin filaments based on the actin-binding domain of utrophin. *Cell Motil. Cytoskeleton.* 64:822–832.

Danilchik, M.V., W.C. Funk, E.E. Brown, and K. Larkin. 1998. Requirement for microtubules in new membrane formation during cytokinesis of *Xenopus* embryos. *Dev. Biol.* 194:47–60.

Fabian, L., and A. Forer. 2007. Possible roles of actin and myosin during anaphase chromosome movements in locust spermatocytes. *Protoplasma.* 231:201–213.

Forer, A., W.T. Jackson, and A. Engberg. 1979. Actin in spindles of *Haemanthus katherinae* endosperm. II. Distribution of actin in chromosomal spindle fibres, determined by analysis of serial sections. *J. Cell Sci.* 37:349–371.

Forer, A., T. Spurck, and J.D. Pickett-Heaps. 2007. Actin and myosin inhibitors block elongation of kinetochore fibre stubs in metaphase crane-fly spermatocytes. *Protoplasma.* 232:79–85.

Gard, D.L., B.J. Cha, and A.D. Roeder. 1995. F-actin is required for spindle anchoring and rotation in *Xenopus* oocytes: a re-examination of the effects of cytochalasin B on oocyte maturation. *Zygote.* 3:17–26.

Garrett, S., K. Auer, D.A. Compton, and T.M. Kapoor. 2002. hTPX2 is required for normal spindle morphology and centrosome integrity during vertebrate cell division. *Curr. Biol.* 12:2055–2059.

Gassmann, R., A. Carvalho, A.J. Henzing, S. Ruchaud, D.F. Hudson, R. Honda, E.A. Nigg, D.L. Gerloff, and W.C. Earnshaw. 2004. Borealin: a novel chromosomal passenger required for stability of the bipolar mitotic spindle. *J. Cell Biol.* 166:179–191.

Goshima, G., R. Wollman, N. Stuurman, J.M. Scholey, and R.D. Vale. 2005. Length control of the metaphase spindle. *Curr. Biol.* 15:1979–1988.

Gruss, O.J., and I. Vernos. 2004. The mechanism of spindle assembly: functions of Ran and its target TPX2. *J. Cell Biol.* 166:949–955.

Gundersen, G.G., and A. Bretscher. 2003. Cell biology. Microtubule asymmetry. *Science.* 300:2040–2041.

Gundersen, G.G., E.R. Gomes, and Y. Wen. 2004. Cortical control of microtubule stability and polarization. *Curr. Opin. Cell Biol.* 16:106–112.

Heasman, J. 2002. Morpholino oligos: making sense of antisense? *Dev. Biol.* 243:209–214.

Homma, K., and M. Ikebe. 2005. Myosin X is a high duty ratio motor. *J. Biol. Chem.* 280:29381–29391.

Homma, K., J. Saito, R. Ikebe, and M. Ikebe. 2001. Motor function and regulation of myosin X. *J. Biol. Chem.* 276:34348–34354.

Kaji, N., A. Muramoto, and K. Mizuno. 2007. LIM-kinase-mediated cofilin phosphorylation during mitosis is required for precise spindle positioning. *J. Biol. Chem.* 283:4983–4992.

Keating, T.J., and G.G. Borisy. 2000. Immunostructural evidence for the template mechanism of microtubule nucleation. *Nat. Cell Biol.* 2:352–357.

Kiehart, D.P., I. Mabuchi, and S. Inoue. 1982. Evidence that myosin does not contribute to force production in chromosome movement. *J. Cell Biol.* 94:165–178.

Kim, N.H., S.K. Cho, S.H. Choi, E.Y. Kim, S.P. Park, and J.H. Lim. 2000. The distribution and requirements of microtubules and microfilaments in bovine oocytes during in vitro maturation. *Zygote.* 8:25–32.

Liu, R., S. Woolner, J.E. Johndrow, D. Metzger, A. Flores, and S.M. Parkhurst. 2008. Sisyphus, the *Drosophila* myosin XV homolog, traffics within filopodia transporting key sensory and adhesion cargos. *Development.* 135:53–63.

Merdes, A., K. Ramyar, J.D. Vechio, and D.W. Cleveland. 1996. A complex of NuMA and cytoplasmic dynein is essential for mitotic spindle assembly. *Cell.* 87:447–458.

Mitchison, T.J., P. Maddox, J. Gaetz, A. Groen, M. Shirasu, A. Desai, E.D. Salmon, and T.M. Kapoor. 2005. Roles of polymerization dynamics, opposed motors, and a tensile element in governing the length of *Xenopus* extract meiotic spindles. *Mol. Biol. Cell.* 16:3064–3076.

Murray, A.W. 1991. Cell cycle extracts. *Methods Cell Biol.* 36:581–605.

Nicklas, R.B., S.C. Ward, and G.J. Gorbsky. 1995. Kinetochore chemistry is sensitive to tension and may link mitotic forces to a cell cycle checkpoint. *J. Cell Biol.* 130:929–939.

O'Brien, L.L., and C. Wiese. 2006. TPX2 is required for postmitotic nuclear assembly in cell-free *Xenopus laevis* egg extracts. *J. Cell Biol.* 173:685–694.

O'Brien, L.L., A.J. Albee, L. Liu, W. Tao, P. Dobrzyn, S.B. Lizarraga, and C. Wiese. 2005. The *Xenopus* TACC homologue, maskin, functions in mitotic spindle assembly. *Mol. Biol. Cell.* 16:2836–2847.

Pecreaux, J., J.C. Roper, K. Kruse, F. Julicher, A.A. Hyman, S.W. Grill, and J. Howard. 2006. Spindle oscillations during asymmetric cell division require a threshold number of active cortical force generators. *Curr. Biol.* 16:2111–2122.

Perez-Moreno, M., C. Jamora, and E. Fuchs. 2003. Sticky business: orchestrating cellular signals at adherens junctions. *Cell.* 112:535–548.

Rodriguez, O.C., A.W. Schaefer, C.A. Mandato, P. Forscher, W.M. Bement, and C.M. Waterman-Storer. 2003. Conserved microtubule-actin interactions in cell movement and morphogenesis. *Nat. Cell Biol.* 5:599–609.

Rosenblatt, J., L.P. Cramer, B. Baum, and K.M. McGee. 2004. Myosin II-dependent cortical movement is required for centrosome separation and positioning during mitotic spindle assembly. *Cell.* 117:361–372.

Sardet, C., F. Prodon, R. Dumollard, P. Chang, and J. Chenevert. 2002. Structure and function of the egg cortex from oogenesis through fertilization. *Dev. Biol.* 241:1–23.

Schloss, J.A., A. Milsted, and R.D. Goldman. 1977. Myosin subfragment binding for the localization of actin-like microfilaments in cultured cells. A light and electron microscope study. *J. Cell Biol.* 74:794–815.

Sharp, D.J., G.C. Rogers, and J.M. Scholey. 2000. Cytoplasmic dynein is required for poleward chromosome movement during mitosis in *Drosophila* embryos. *Nat. Cell Biol.* 2:922–930.

Sokac, A.M., C. Co, J. Taunton, and W. Bement. 2003. Cdc42-dependent actin polymerization during compensatory endocytosis in *Xenopus* eggs. *Nat. Cell Biol.* 5:727–732.

Sun, Q.Y., L. Lai, K.W. Park, B. Kuhholzer, R.S. Prather, and H. Schatten. 2001. Dynamic events are differently mediated by microfilaments, microtubules, and mitogen-activated protein kinase during porcine oocyte maturation and fertilization in vitro. *Biol. Reprod.* 64:879–889.

Tokuo, H., K. Mabuchi, and M. Ikebe. 2007. The motor activity of myosin-X promotes actin fiber convergence at the cell periphery to initiate filopodia formation. *J. Cell Biol.* 179:229–238.

Toyoshima, F., and E. Nishida. 2007. Integrin-mediated adhesion orients the spindle parallel to the substratum in an EB1- and myosin X-dependent manner. *EMBO J.* 26:1487–1498.

Waterman-Storer, C., D.Y. Duey, K.L. Weber, J. Keech, R.E. Cheney, E.D. Salmon, and W.M. Bement. 2000. Microtubules remodel actomyosin networks in *Xenopus* egg extracts via two mechanisms of F-actin transport. *J. Cell Biol.* 150:361–376.

Weber, K.L., A.M. Sokac, J.S. Berg, R.E. Cheney, and W.M. Bement. 2004. A microtubule-binding myosin required for nuclear anchoring and spindle assembly. *Nature.* 431:325–329.

Wittmann, T., M. Wilm, E. Karsenti, and I. Vernos. 2000. TPX2, A novel *Xenopus* MAP involved in spindle pole organization. *J. Cell Biol.* 149:1405–1418.

Zhou, J., K. Gupta, J. Yao, K. Ye, D. Panda, P. Giannakakou, and H.C. Joshi. 2002. Paclitaxel-resistant human ovarian cancer cells undergo c-Jun NH2-terminal kinase-mediated apoptosis in response to noscapine. *J. Biol. Chem.* 277:39777–39785.